Supplementary Information (SI) for Journal of Materials Chemistry A.

Supporting Information

Poly(naphthalene-co-biphenyl piperidinium) based highly conductive and durable anion exchange membrane for electrochemical energy devices

Avoy Mondal and Bijay P Tripathi*

Functional Materials and Membranes Laboratory, Department of Materials Science & Engineering, Indian Institute of Technology Delhi, New Delhi, 110016, India

Phone: +91-11-26597364, Email: bptripathi@mse.iitd.ac.in; drbptripathi@gmail.com

Table of contains

S1. Materials

Biphenyl (>99.5%) and Naphthalene (>98%) were purchased from TCI, Japan. N-methyl-4-piperidone (>96.5%), Trifluoroacetic acid (>99%), Trifluoromethane sulfonic acid (TFSA; >98%), and DMSO-d_6 (99.96 at% D) were purchased from Sigma Aldrich, USA. Methyl iodide (99%), N-methyl pyrrolidone (NMP; reagent grade), dimethyl sulfoxide (DMSO; reagent grade), Ethyl acetate, NaOH (99% pellets, VWR), and K_2CO_3 were purchased from CDH, India and used as received. Millipore water was used for all purposes.

S2. Preparation of anion exchange membrane

S2.1. Synthesis of poly(naphthalene-biphenyl piperidine) copolymer

The poly(naphthalene-biphenyl piperidine) (PNBM) copolymer was synthesized via a superacid-catalyzed Friedel-Crafts polymerization.[1] Biphenyl (3.08 g, 20 mmol) and naphthalene (0.683 g, 5.33 mmol) were dissolved in anhydrous dichloromethane (1.2 ml) in a 100 ml round bottom flask, followed by the addition of N-methyl piperidone (3.22 ml, 27.73 mmol). The reaction solution was purged with N_2 for 10 minutes to remove air and moisture. To control fume generation, trifluoroacetic acid (TFA, 3.646 mL, 47.62 mmol) was added slowly. Subsequently, trifluoromethanesulfonic acid (TFSA, 24.325 mL, 0.275 mol) was introduced when the reaction temperature reached ~0 ºC. Upon TFSA addition, the solution color changed from light-yellow to red. The reaction temperature was maintained at 0 °C by using a chiller to avoid product elimination. The reaction mixture became highly viscous after 8-9 hours, making stirring difficult. After reaching the desired viscosity, the reaction was continued for an additional hour before being quenched in a 1 M aqueous NaOH solution to precipitate the polymer. The resulting white fibrous polymer was filtered, neutralized by washing with deionized water, and dried in an oven at 80 ºC for 24 hours. The reaction yield was approximately 95.6%.

S2.2. Quaternization of poly (naphthalene-biphenyl piperidine) polymer

In a 100 ml round bottle flask, the PNBM polymer (6.0 g, 24.6 mmol) was dissolved in DMSO (60 mL), and TFA (3 ml) was added as a cosolvent. Upon the addition of TFA, the polymer solution became clear. The homogenous PNBM solution was then treated with K_2CO_3 (6.14 g, 44.493 mmol) and iodomethane (5.24 ml, 84.19 mmol). The quaternization reaction was carried out for 48 h at room temperature. Afterward, the polymer solution precipitated in ethyl acetate (150 ml) and thoroughly rinsed with DI water several times to remove any residual iodomethane and K_2CO_3. The final product was dried at 80 °C for 24 h, yielding 94% of the quaternary polymer (QPNBM).

S2.3. Membrane casting and ion exchange

The QPNBM membrane was made using a solution-casting method. First, 2g of QPNBM was dissolved in 6.67 ml DMSO to obtain a 30 wt.% polymer solution. The solution was degassed before casting to eliminate any trapped air bubbles. The degassed, colorless solution was then cast onto a glass plate using automated film-casting equipment set to a gap height of 15 mm and a casting speed of 15 mm/s. After casting, the film was allowed to slowly dry under ambient conditions for 48 h. It was then subjected to drying in an oven at 35 °C for 24 hours, 40 °C for an additional 24 hours, and finally 80 ºC for 12 h to ensure complete solvent removal. The fully dried membrane was brought to RT and subsequently hydrated in deionized water, allowing it to be peeled from the glass plate. The process resulted in a 315 cm^2 with a thickness of 14 ± 2 μm transparent membrane in iodide form. A larger membrane (400 cm^2) with a thickness of 90 ± 5 μm was also produced, which remained flexible at ambient temperature. Ion exchange from iodide to hydroxide or chloride form was achieved by immersing the membranes in 1 M KOH or 1 M KCl for 24 hours at RT. After ion exchange, the membranes were rinsed multiple times with deionized water to remove any remaining base or salt before being dried in the oven.

S3. Characterization and measurements

S3.1. Structural characterization of polymer and membrane

The chemical structures of the PNBM and cationic QPNBM co-polymers were determined using ^1H NMR spectroscopy on a Bruker 500 MHz spectrometer (Bruker advance AV-III). DMSO-d^6 was used as the solvent along with 3-4% TFA to shift the water peak from 3.34 ppm to 12-14 ppm.[2] The Attenuated Total Reflectance-Fourier Transform Infrared spectroscopy (ATR-FTIR) of PNBM co-polymer and QPNBM membrane was performed on a Nicolet 6700 spectrometer (Thermo Scientific, USA) in the 4000-400 cm^{-1} range. The intrinsic viscosity ($[\eta]$) of PNBM and QPNBM was evaluated using an Ubbelohde viscometer after dissolving the polymer in DMSO solution (0.1 M) at 30 °C. The efflux time of each sample was measured three times at four different concentrations. The reduced viscosity (η_{red}) and inherent viscosity (η_{inh}) were then calculated using the following equations:

Reduced viscosity (η_{red}) = $\frac{\frac{t_s}{t_b}-1}{c}$ (1)

Inherent viscosity (η_{inh}) = $\frac{ln\,(\frac{t_s}{t_b})}{c}$ (2)

where, t_s is the efflux time for the polymer solution at concentration c, and t_b is the efflux time of the solvent. The intrinsic viscosity ([η]) of the PNBM solution was determined from the intersection of the plot at the axis derived from the extrapolation of η_{red} and η_{inh} at c = 0. The rheological behavior of the polymer solution was investigated using a parallel plate C-VOR 150 digital rheometer (Bohlin Instruments). A temperature sweep was performed on a 10% QPNBM polymer solution, with a heating rate of 5 °C/minute from 30-120 °C to evaluate its viscoelastic properties under varying thermal conditions.

S3.2. Membrane morphology

Field emission scanning electron microscopy (FE-SEM) (Jeol JSM-7800F Prime FESEM) was used to acquire the surface and cross-section morphologies of the QPNBM membrane. Cross-sectional samples were prepared by cryo-fracturing the membrane in liquid nitrogen. Before imaging, all samples were sputter-coated with a thin gold layer (~ 6 nm) using the Jeol JEC-3000FC auto fine coater. Elemental composition and mapping were performed through energy dispersive X-ray (EDX) analysis using an Oxford SDD X-max 80 EDS detector. In addition, high-resolution transmission electron microscopy (HR-TEM) and atomic force microscopy (AFM, Bruker Nano Inc, ICON IR) were used to further investigate the phase-separated morphology of the QPNBM membrane. The HR-TEM specimens were prepared by drop casting 1% QPNBM solution (in DMSO) into a copper grid kept 24 h for air drying. After that, the copper gride was immersed in 0.5 M aqueous Na_2WO_4 solution for 12 h, then washed with deionized water and dried at room temperature for 24 h for TEM analysis. For AFM analysis, a silicon tip (0.4 N/M force constant) was used to scan the membrane surface in tapping mode. The small angle X-ray scattering (SAXS) analysis of the dry QPNBM membrane in I^- form was carried out using the Anton Paar SAXS point 2.0 system, equipped with 2D EIGER R series hybrid photon counting (HPC) detectors with HR WAXS module. The Scattering vector at maximum intensity (q_{max}) was calculated using the following equation:

$$q_{max} = \frac{4\pi\,sin\theta}{\lambda} \quad (3)$$

where, λ is the wavelength of the Cu K(α) radiation and 2θ is the scattering angle.

The separation between the ionic clustered (d) was calculated using the Bragg law with the help of the following equation.

$$d = \frac{2\pi}{q_{max}} \quad (4)$$

S3.3. Pore size estimation

The surface area, pore size, and pore distribution of the QPNBM membrane were evaluated using nitrogen adsorption/desorption isotherms at 77 K and were investigated using a Quantachrome instrument (model Autosorb iQ-XR-AG-AG). Before analysis, the sample was dried in an air oven at 80 ºC. A rod cell with a 9 mm outer diameter was used to contain the sample and 29.6 mg of the QPNBM membrane was degassed at 100 ºC for 10 hours to remove any moisture or impurities. The nitrogen isotherm was generated over 20-20 points during a 10-hour period in a liquid nitrogen bath. The specific surface area was calculated using the Brunauer-Emmett-Teller (BET) model, and the pore size distribution (including pore size and pore volume) was determined using the Density Functional Theory (DFT) method, derived from the desorption curve of the isotherm.

S3.4. Water uptake, swelling, and surface charge measurements

The water uptake for the QPNBM membranes in both iodide and hydroxide forms was measured at temperatures ranging from 30 to 80 °C. Membranes were equilibrated for 24 h at each temperature stage to ensure thorough hydration and the hydrated membranes were consistently used to obtain high-temperature results. Test samples (2×2 cm^2) were initially dried at 80 °C in an oven until a constant mass (W_{dry}) was achieved. After drying, the wet weight (W_{wet}) along with their dimensions (thickness and length) were recorded following immersion in DI water. Before weighing, excess surface water was carefully removed using dry filter paper. The water uptake and swelling ratios of the membranes were calculated using the following equations:

$$\text{Water uptake (WU, \%)} = \frac{W_{wet} - W_{dry}}{W_{dry}} \times 100\% \quad (5)$$

$$\text{Swelling ratio (SR, \%)} = \frac{L_{wet} - L_{dry}}{L_{dry}} \times 100\% \quad (6)$$

where, W_{wet}, L_{wet} and W_{dry}, L_{dry} denotes the weight and dimension after soaking in water and dry conditions, respectively.

The zeta potential (ζ) of the QPNBM membrane was measured in a 1 mmol/L KCl aqueous electrolyte solution over a pH range of 9 to 3. The pH was adjusted using automatic titration with a 0.05 mol/L HCl solution. For each pH value, two rinsing cycles and four zeta potential measurements were performed to ensure accuracy. The change in streaming potential/current as a function of pH was recorded using two electrodes. The zeta potential (ζ) was calculated with the help of the Helmholtz–Smoluchowski formula, as shown as follows:

$$\zeta = \frac{dI_{str.}}{d\Delta p} \times \frac{\eta}{\varepsilon_e \times \varepsilon_0} \times \frac{L}{A} \tag{7}$$

where, $I_{str.}$, Δp, η, ε_e, ε_0 , L and A are streaming current, hydrodynamic pressure difference across the membrane, the viscosity of the dielectric solution, the dielectric constant of the electrolyte solution, vacuum permittivity, streaming channel length, and streaming channel cross-section, respectively.

S3.5. Ion exchange capacity, hydration number, and state of water measurement

The ion-exchange capacity (IEC) of the QPNBM membrane was determined using the Mohr titration method. First, the ion exchange was performed by immersing the dry membrane in its Cl^- form in a 1 M KNO_3 solution (25 ml) for 48 hours. The solution was then titrated with 0.01 M $AgNO_3$, using K_2CrO_4 as an indicator. The endpoint was confirmed by the formation of a red precipitate of Ag_2CrO_4. The dry mass of the membrane in OH^- form was estimated using the equation $W_{OH^-} = W_{Cl^-} - 0.1844V_{AgNO_3}$,[3,4] where V_{AgNO_3} is the volume (L) of $AgNO_3$ consumed. The IEC (mmol/g) was then calculated using the following equation:

$$IEC_{Cl^-/OH^-} = \frac{V_{AgNO_3} \times S_{AgNO_3}}{W_{dryCl^-/OH^-}} \tag{8}$$

where, W_{dryCl^-/OH^-} is the dry mass of the membrane in Cl^- or OH^-form (g). V_{AgNO_3} (L) and S_{AgNO_3} (mol/L) are the volume and concentration of $AgNO_3$ solution, respectively.

The hydration number (λ) represents the number of water molecules associated with each quaternary ammonium group in the membrane, calculated using the equation below.

$$\lambda = \frac{WU \times 10}{IEC \times 18} \tag{9}$$

where, WU is the percentage water uptake value of the membrane.

The Differential Scanning Calorimetry (DSC) was used to determine the number of free water (N_{free}) and bound water (N_{bound}) per ionic group in the OH^- form of the membrane. The experiment was performed by first cooling the membrane up to -50 °C heating followed by heating from -50 to 20 °C with a rate of 4 °C/min in a nitrogen environment. The amount of freezing water in the equilibrated membrane was calculated using the following equation:[5]

$$N_{free} = \frac{H_f / H_{ice}}{(M_{wet} - M_{dry})/M_{wet}} \times \lambda \qquad (10)$$

where, H_f is the total freezing enthalpy obtained from the freezing peak of the DSC histogram. H_{ice} is the fusion enthalpy of the water. M_{wet} and M_{dry} are the wet and dry weight of the membrane, respectively. λ is the equilibrium water contained in the membrane.

$$H_{ice} = H^0{}_{ice} - \Delta C_P \Delta T_f \qquad (11)$$

where, $H^0{}_{ice}$ is the enthalpy of melting of the pure bulk ice (333.5 J/g), ΔC_P is the specific heat capacity difference between water and ice, and ΔT_f is the freezing point depression. The non-freezable bound (N_{bound}) water was calculated by subtracting N_{free} from the equilibrated water content (λ).

S3.6. Ionic conductivity

The conductivity of Cl^- and OH^- ions in the QPNBM membrane was measured using a two-electrode AC impedance analyzer on an electrochemical workstation (Biologic VSP3). The test samples were equilibrated in 1 M KCl and 1 M KOH solutions for 24 h to facilitate ion exchange of the respective ions. After equilibration, the membranes were placed between two stainless-steel plates and tested over a frequency range of 0.1 Hz to 0.1 MHz. All measurements were conducted under 100% humidity at temperatures ranging from 30 °C to 100 °C. To prevent the formation of bicarbonate, OH^- ion conductivity was measured in a N_2 atmosphere. The ionic conductivity was calculated using the following equation:

$$\sigma = \frac{L}{A \times R} \qquad (12)$$

where, L and A are the thickness (measured using a digital Mitutoyo micrometer) and cross-section area of the test membrane, respectively. R is the membrane resistance as determined by the impedance study. The equilibrated membrane thickness (L) was utilized for the conductivity calculation.

S3.7. Hydroxide ion permeation and ion transport number

The hydroxide ion permeability through the anion exchange membrane was measured using a custom-built two-chamber diffusion cell. A 50 ml 3 M KOH solution was added to the feed side, while 50 ml of Millipore water was placed on the permeate side. The hydroxide ion permeation through the soaked membrane (area = 6.15 cm^2) was monitored by measuring the pH (Mettler Toledo pH meter) on the permeate side at regular intervals at ambient temperature. The hydroxide ion concentration (C_{OH^-}) was calculated from measured pH data using the following equation:

$$pH = 14 - \log(C_{OH^-}) \tag{13}$$

Similarly, the permeability of the dimethyl viologen (MV^{2+}) ion was determined by using 50 ml (0.015 M) aqueous solution in the feed and 50 ml Millipore water in the permeate side in the diffusion cell. Both chambers were continuously stirred to minimize concentration polarization at the membrane surface. The concentration of the MV^{2+} in the permeate side was measured by UV-vis spectroscopy at ~256 nm. The hydroxide ion and MV^{2+} permeability were calculated by considering the pseudo-steady state condition of the two reserves, using the following equations:[6]

$$V_B \frac{dc_B}{dt} = \frac{AP}{L}(C_A - C_B) \tag{14}$$

$$\ln\left(\frac{C_A}{C_A - C_B}\right) = \frac{AP}{LV_B} t \tag{15}$$

where, A (cm^2) and L (cm) are the effective area and thickness of the membrane, respectively, V_B (ml) is the permeate side volume, C_B (mol/L) is the concentration of hydroxide or MV^{2+} ion at the permeate side at time t (s) and C_A (mol/L) is the initial concentration of the hydroxide or MV^{2+} ion on the feed side, respectively. Permeability P (cm^2/s) was measured from the slope of the $\ln\left(\frac{C_A}{C_A - C_B}\right)$ vs. t curve.

The hydroxide ion transport number (t_m) through the QPNBM was determined using membrane potential (E_m) measurement in a 0.1/1 M KOH concentration gradient. The t_m was calculated using the following equation:[7,8]

$$E_m = (2t_m - 1)\frac{RT}{F}\ln\left(\frac{a_1}{a_2}\right) \tag{16}$$

where, R (8.314 Jmol^{-1} K^{-1}) is the gas constant, T (K) is the absolute temperature, F (94085 JV^{-1} mol^{-1}) is the Faraday constant, a_1 and a_2 are the activity of high and low concentration solution, respectively.

S3.8. Thermal stability

The thermal degradation characteristics of the QPNBM membrane were examined using a thermogravimetric analyzer (TGA Q500, TA instrument). Before analysis, the samples were dried at 80 °C for 24 hours to remove residual moisture. The analysis was conducted under a N_2 atmosphere over a temperature range of 30 to 750 °C at a heating rate of 10 °C/min. The glass transition temperature (T_g) was measured using differential scanning calorimetry

(DSC, Q2000 TA equipment) in an N_2 environment at a heating rate of 10 °C/min. The T_g value was calculated using the inflection point of the second heating scan.

S3.9. Mechanical properties and rheology

The temperature-dependent mechanical behavior of the QPNB membrane was investigated using a dynamic mechanical analyzer (DMA, Q800 TA instruments). The test was conducted in an N_2 atmosphere at temperatures ranging from 100 to 400 ºC, with a scan rate of 4 ºC/minute. The test sample, sized 0.6×3.7 cm, was secured in the tension grip of the DMA. At a frequency of 1 Hz and an applied preload force of 0.01 N, the storage modulus (E'), loss modulus (E''), and damping factor (tan δ) were measured. To assess the tensile strength and elongation at break, a universal testing machine (UTM) with a 1 KN load cell was employed. The experiment was conducted under ambient conditions using a membrane sample sized 0.8×4 cm, stretched at a rate of 1 mm/min. Additionally, the rheological behavior of the QPNBM polymer solution was examined using a parallel plate C-VOR 150 digital rheometer (Bohlin Instruments). A temperature sweep was performed on the QPNBM polymer solution to evaluate the viscosity change in the polymer solution.

S3.10. Alkaline stability

The stability of the QPNBM membrane was assessed using ^{1}H NMR spectroscopy and the OH^- conductivity measurements. The membrane's OH^- ion conductivity trend was monitored by storing it in 1 M KOH at 80 °C for a total duration of 1512 hours. Conductivity measurements were taken at specific intervals, including the initial measurement, and after 1008 hours and 1512 hours of alkali exposure. To assess any structural changes due to prolonged alkali exposure, the alkali-treated membrane was subjected to ion exchange into its Br^- form, after which its ^{1}H NMR spectrum was recorded. This allowed for the identification of any chemical degradation or modifications in the polymer structure over time.

S4. Fabrication of membrane electrode assembly for AEMWEs

A catalyst-coated QPNBM membrane was sandwiched between two stainless steel bipolar plates (thickness 3 mm) to produce the membrane electrode assembly (MEA). The titanium felt (0.2-0.5 mm, 55% porosity, Fuel Cell Store, USA) was used as the anodic gas diffusion layer, whereas the cathodic gas diffusion layer was carbon paper (AvCarb MGL190, Fuel Cell Store, USA). Parallel flow channels of 1.5 mm depth and 1.5 mm wide were created on bipolar plates for better mass flow. For MEA preparation, anion-exchange QPNBM polymer was utilized as the ionomer. Iridium oxide (IrO_2, Alfa Aesar Co., USA) was utilized as the anode catalyst and platinum (Pt/C, 50% Platinum on Vulcan XC 72 Carbon, Fuel Cell Store, USA) was employed as the cathodic catalyst. The anode catalyst ink was prepared by dissolving 17.6 mg of IrO_2 in 24 mg of ethanol, 12 mg of DI water, and 19.5 µl of 10% QPNBM/DMSO ionomer solution. Similarly, the cathodic catalyst ink was obtained by mixing 6.4 mg 50 wt.% Pt/C and 16 µl of 10% QPNBM/DMSO ionomer solution in 26 mg ethyl alcohol and 13 mg DI water. Before coating, the QPNBM membrane was immersed in 1 M KOH solution for 12-15 hours to complete the ion exchange process, followed by washing with distilled water to remove surface salts. The catalyst slurries, which were magnetically stirred and sonicated for 1 hour under ice-cold conditions, were then manually brush-coated onto both sides of the membrane. The layers were allowed to dry at room temperature for 24 hours. This procedure achieved catalyst loadings of 2 mg/cm^2 for Ir at the anode and 0.5 mg/cm^2 for Pt at the cathode, with ionomer loadings of 10% and 20%, respectively. The EIS of the electrolyzer was conducted at 1.6 V over a frequency range of 0.5 MHz to 0.5 Hz, with an amplitude of 16 mV. All electrochemical measurements were performed on an Autolab M204 potentiostat/galvanostat with a 10 A current booster. For running the AEMWE, a 1M KOH electrolyte solution was circulated at a 20 ml/min flow rate on the anode side at 60 $^{\circ}$C through the parallel flow channels on the bipolar plate (active area: 6.2 cm^2). The single-cell AEMWE test was performed using the voltage sweep method at a scan rate of 10 mV/s, within the voltage range of 1.2 to 2 V.

S5. Aqueous redox flow battery testing

The aqueous redox flow battery (RFB) test was conducted in a redox-flow cell framework (Scribner Associates Inc.) with an active area of 25 cm^2, utilizing methyl viologen (MV) as the anolyte and (Ferrocenylmethyl) trimethylammonium chloride (FcNCl) as the catholyte. The electrodes, made from SIGRACELL® graphite felt, were pre-treated by heating in air at 400 °C for 4 hours prior to the assembly of the single cell. The QPNB membrane separator between the anolyte and catholyte chambers, was pre-soaked in 0.1 M NaCl solution to optimize its ion exchange properties. 10 mL of 0.5 M MV and 0.5 M FcNCl (both in 2 M NaCl) were circulated in respective chambers at a flow rate of 40 mL/min. The whole setup was flushed with N_2, and the system was enclosed in a custom N_2 compartment to maintain an inert atmosphere. The charge and discharge performance of the flow battery was evaluated across a voltage window of 0.1 to 1.5 V, with current densities ranging from 10 to 40 mA/cm^2 using a VSP-3e biologic instrument under an N_2 environment at 30 °C temperature. The EIS of the battery cell was measured within a frequency range of 300 MHz to 100 Hz, with 10 points per decade. The area-specific resistance (ASR) was calculated by multiplying the active area of 25 cm^2 by the actual component impedance from the Nyquist plot.

S6. ^{1}H NMR spectroscopy of PNBM polymer in progressive reaction times

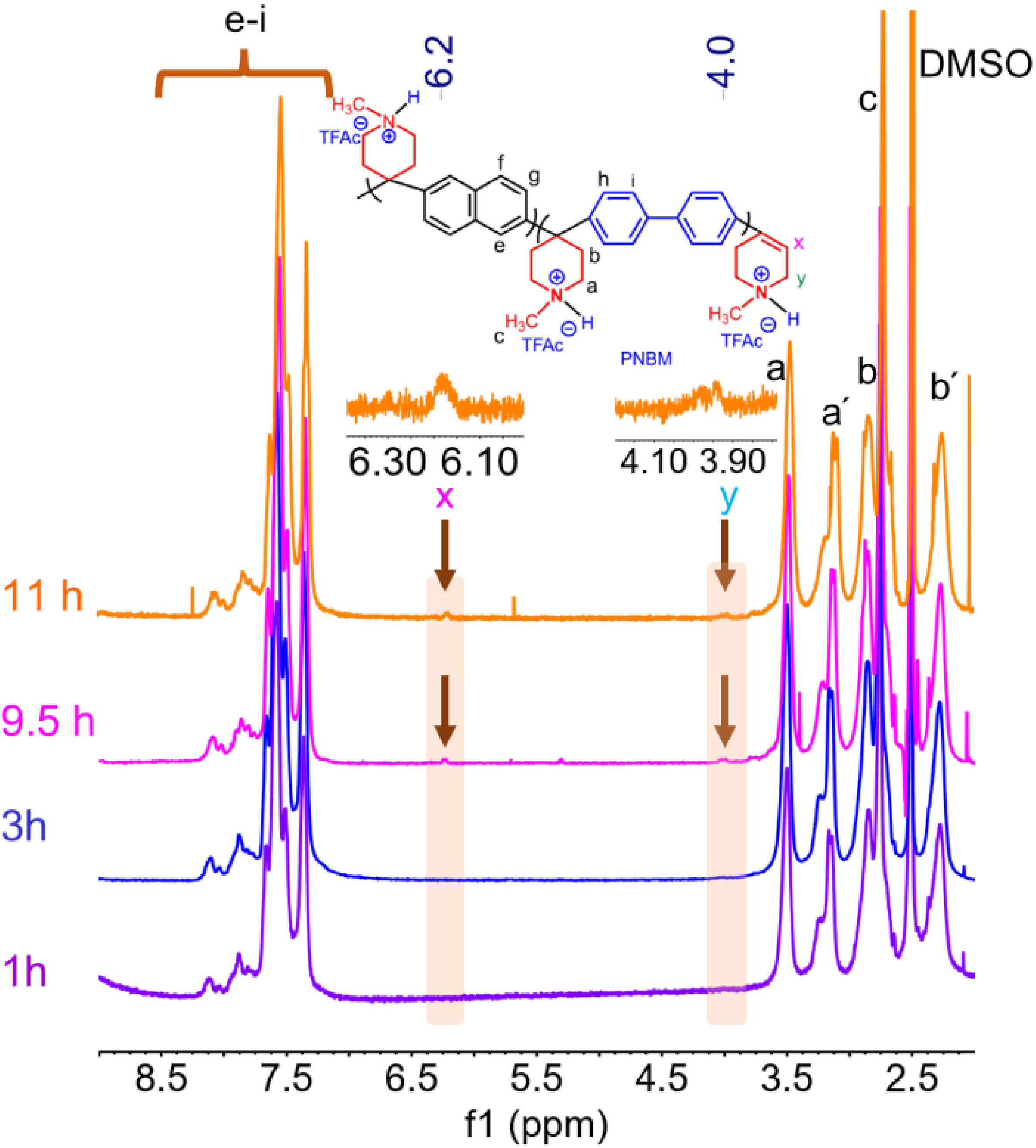

Figure S1. ^{1}H NMR spectroscopy of the PNBM polymer during the progressive polycondensation reaction demonstrated that the concentration of unsaturated chain ends increased with prolonged reaction time, as shown by the protonic signals of x and y at 6.2 and 4 ppm, respectively.

S7. ATR-FTIR of PNBM and QPNBM polymer

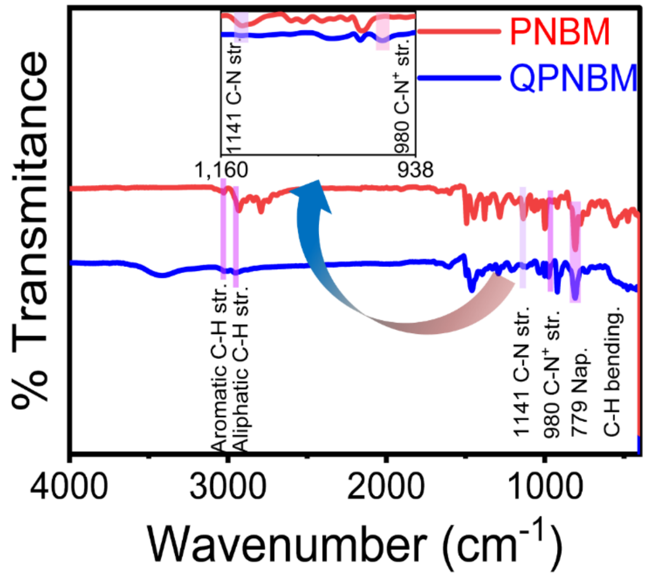

Figure S2. ATR-FTIR spectra of PNBM and QPNBM, highlighting characteristic absorption bands corresponding to aliphatic and aromatic C–H stretching, C–N, and C–N$^+$ vibrations.

S8. ^{1}H NMR spectroscopy

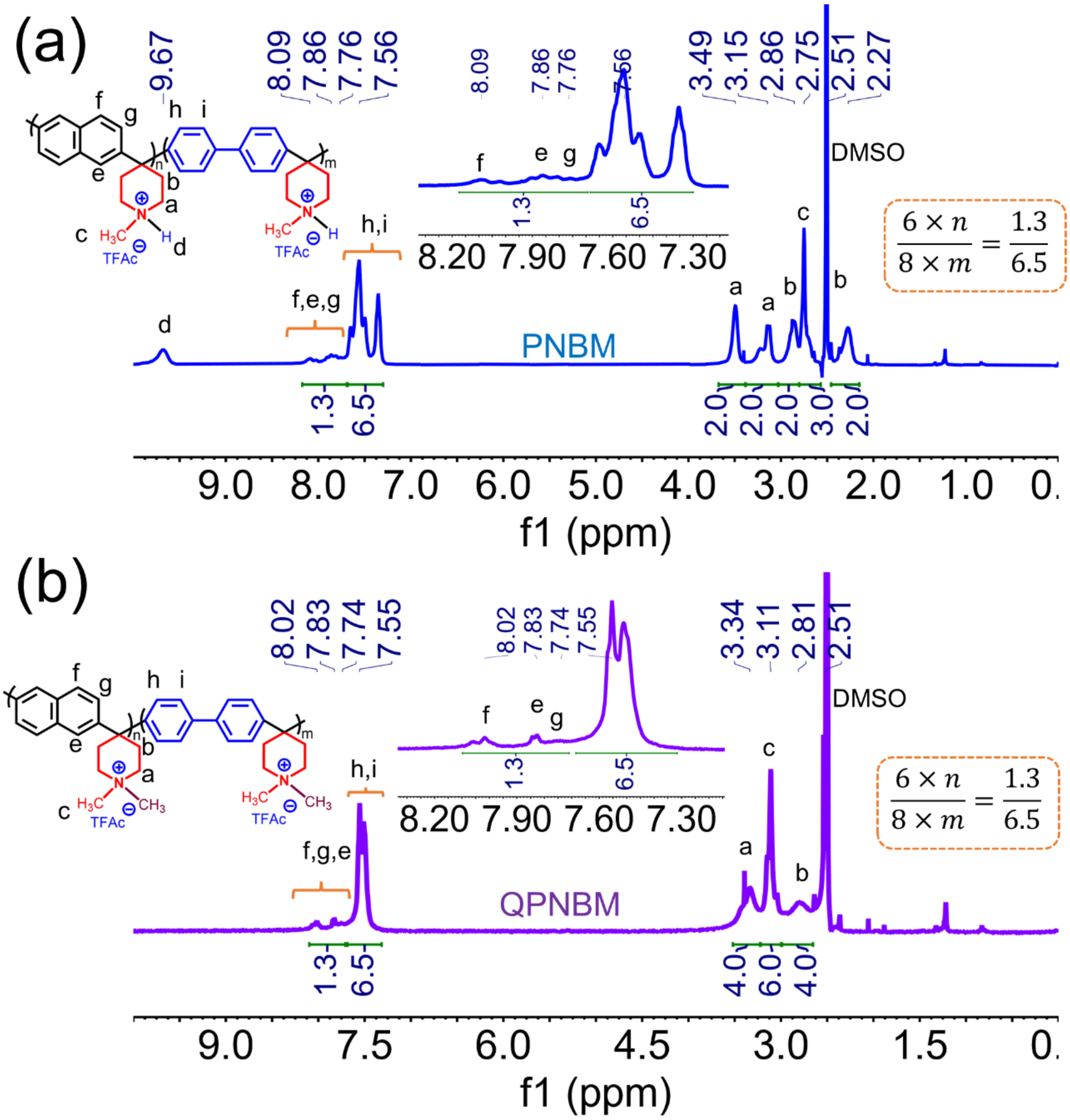

Figure S3. ^{1}H NMR spectral analysis of PNBM and QPNBM polymers reveals a notable transformation in the methylene proton peak distribution. Initially, the PNBM polymer displays four discrete methylene proton signals. Upon quaternization, these signals coalesce into two distinct methylene proton peaks in the QPNBM polymer spectrum. This modification can be attributed to the heightened symmetry of the electrical environment surrounding the nitrogen atom within the piperidine moiety.

S9. Rheology study

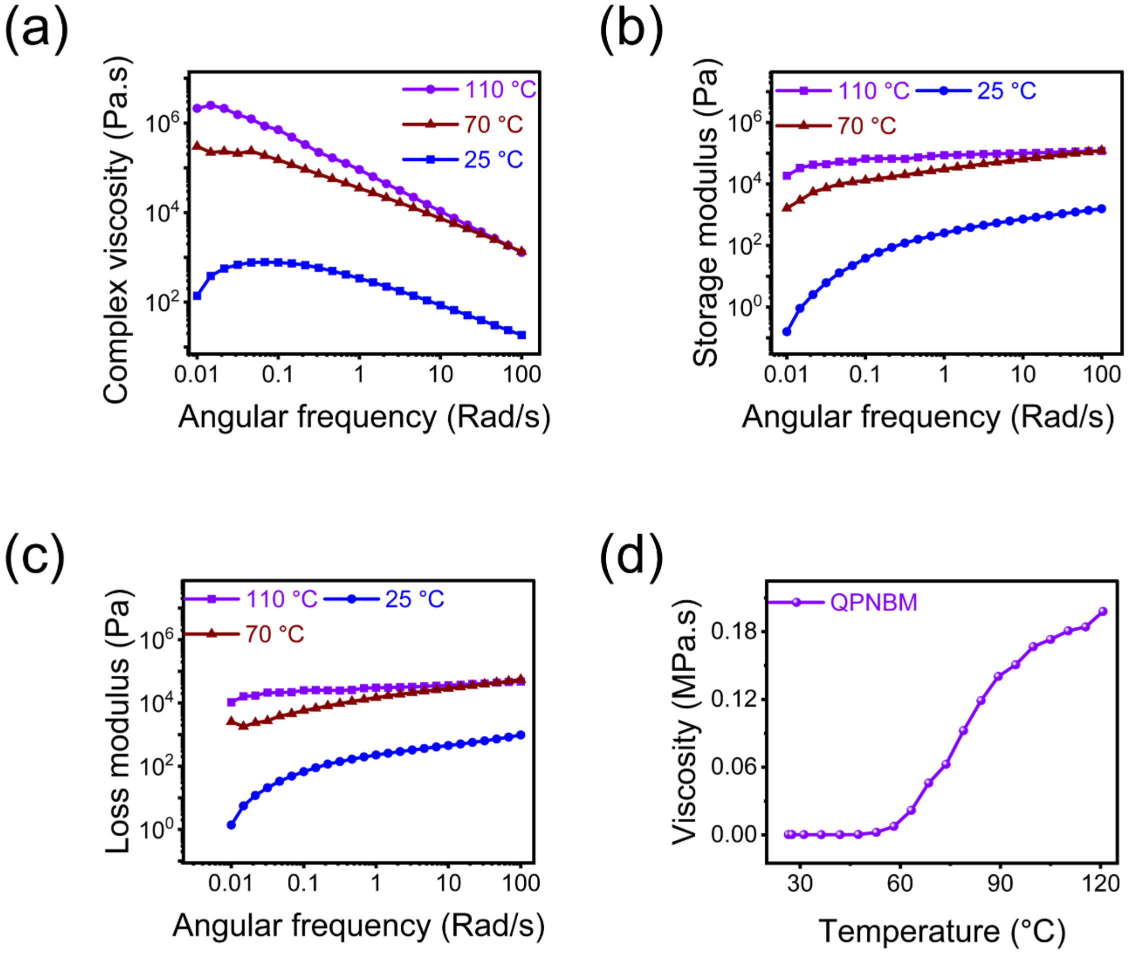

Figure S4. (a) Complex viscosity of the QPNBM polymer solution as a function of angular frequency at different temperatures; (b) storage modulus and (c) loss modulus of the QPNBM polymer as a function of angular frequency at different temperatures. (d) Temperature effect on the viscosity of 10 wt.% QPNBM polymer.

S10. Elemental mapping & analysis

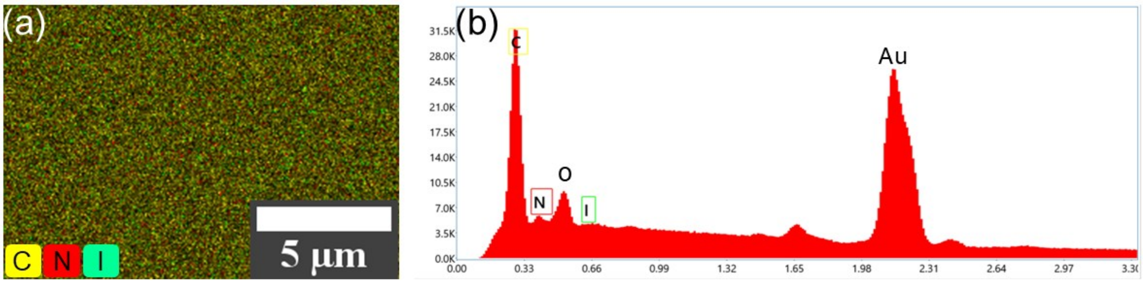

Figure S5. (a) Elemental mapping of QPNBM in I^- form and (b) Elemental analysis of QPNBM in its I^- form. The prominent Au peak detected at 2 was attributed to the thin conductive coating applied to the membrane. The oxygen and gold peaks were subsequently omitted during the acquisition of the mapping spectrum.

Table S1. Elemental analysis of QPNBM membrane.

Element	Weight %	Atomic %	Error %
C K	93.9	96.1	7.2
N K	4.3	3.8	15.1
I M	1.8	0.2	9.9

S11. Characterization of membranes using AFM and small angle X-ray diffraction

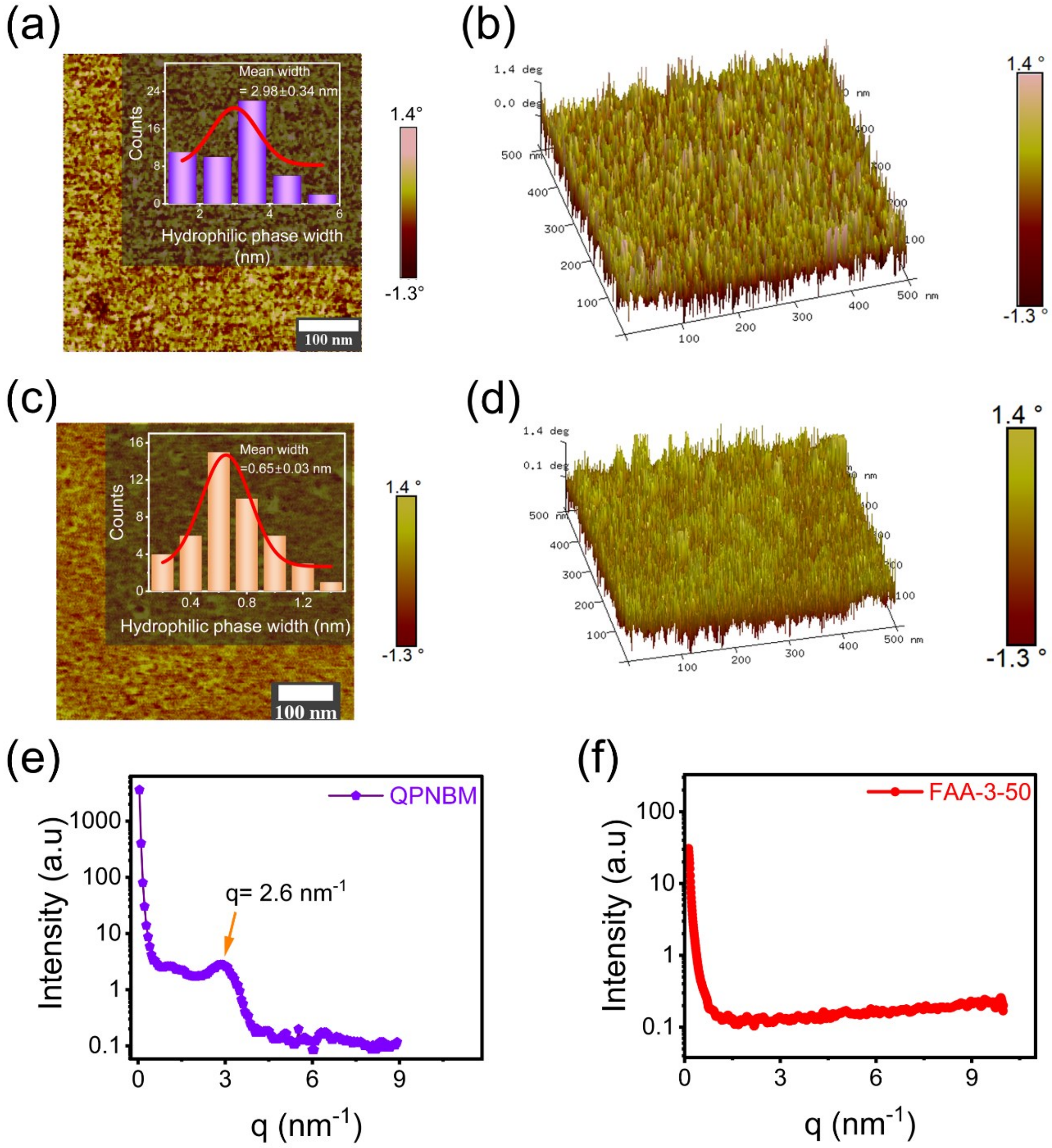

Figure S6. (a) Two-dimensional AFM phase image in iodide form, illustrating phase separation with hydrophilic and hydrophobic domains of the QPNBM membrane, (b) Three-dimensional phase image of the QPNBM membrane in I^- form, (c) Two-dimensional AFM phase image of the FAA-3-50 membrane in Br^- form, (d) Three-dimensional phase image of the FAA-3-50 membrane in Br^- form, (e) Small-angle X-ray scattering (SAXS) profile of the QPNBM membrane indicating a maximum scattering vector of 2.6 nm^{-1}, (f) SAXS profile of the FAA-3-50 membrane reveals the absence of a maximum scattering vector.

S12. Surface charge analysis

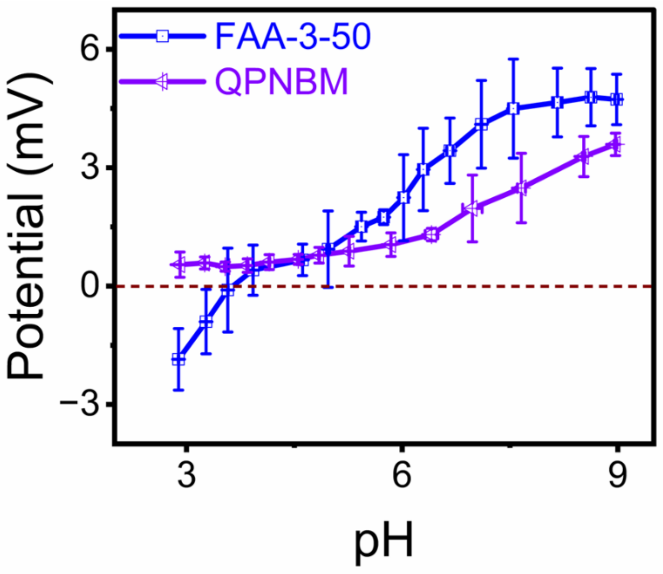

Figure S7. Zeta potential of QPNBM and FAA-3-50 membranes.

S13. Water uptake, swelling, thermal, and mechanical properties

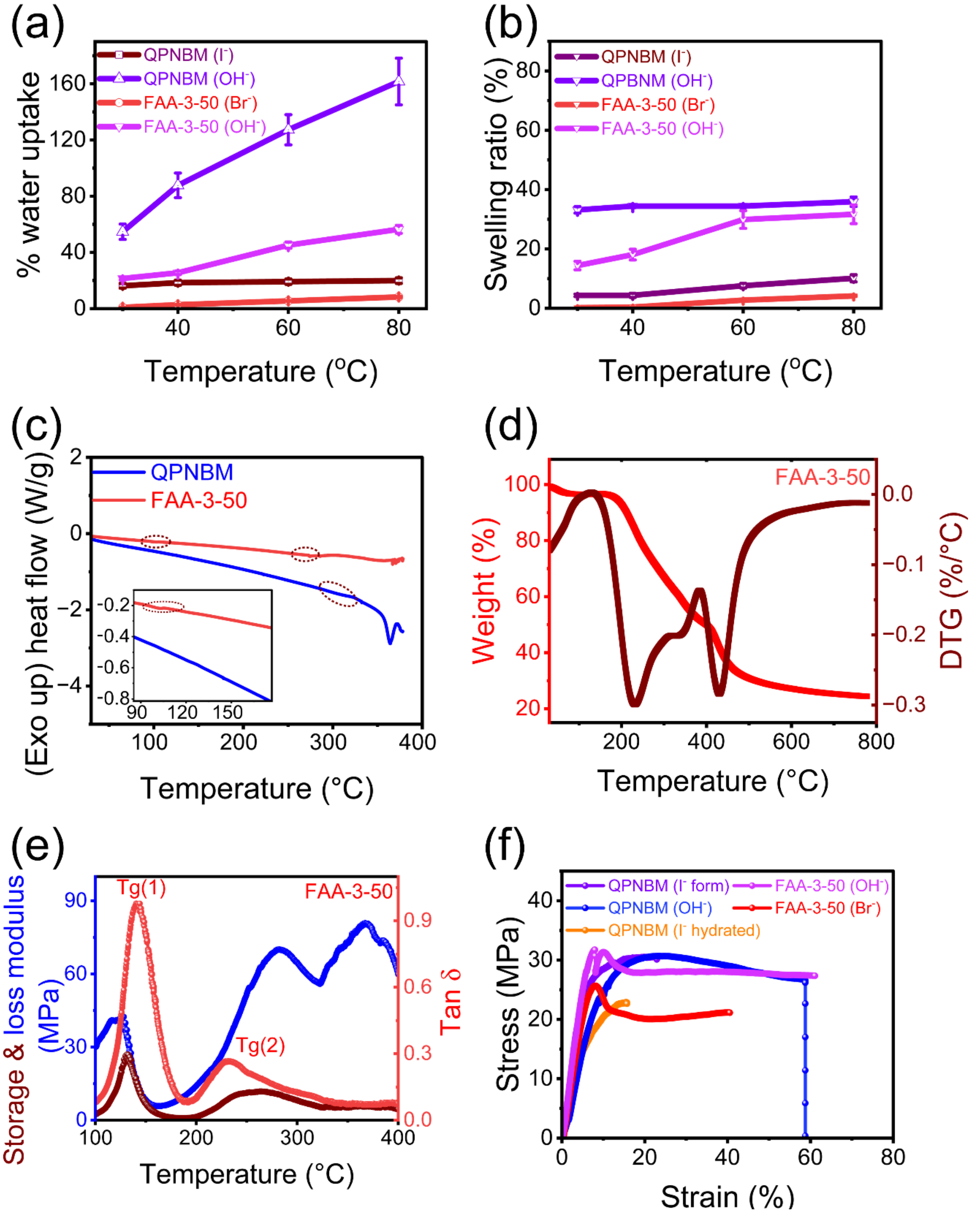

Figure S8. (a) Water uptake and (b) swelling ratio of the QPNBM and FAA-3-50 membranes as a function of temperature. (c) DSC curve indicating the glass transition temperature of QPNBM and FAA-3-50 membranes, (d) TGA and DTA curves showing thermal stability and degradation steps of the FAA-3-50 membrane, (e) DMA curve depicting the storage and loss moduli variation with temperature of the FAA-3-50 membrane, and (f) Stress-strain curve of the QPNBM and FAA-3-50 membranes at room temperature.

S14. Low-temperature DSC plot

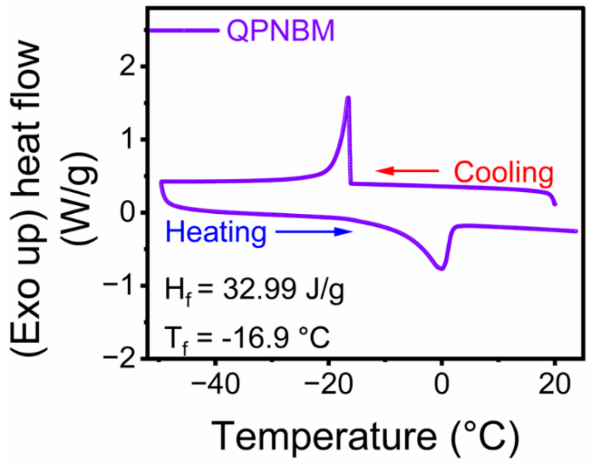

Figure S9. DSC cooling and heating thermograms of the QPNBM membrane.

S15. Ion exchange capacity, hydration number, and state of water

Table S2. The ion exchange capacity, hydration number, total freezing enthalpy (H_f), freezing point depression (ΔT_f), equilibrated water contains (λ), number of free waters per ionic side (N_{free}), and number of bound waters per ionic side (N_{bound}) of QPNBM and FAA-3-50 membrane.

Sample	*IEC (mmol/g)*			*Hydration number (λ) (30 °C)*		H_f *(J/g)*	ΔT_f	N_{free}	N_{bound}
	Titration (Cl^-)	*Titration (OH^-)*	*NMR (I^-)*	*I^- form*	*OH^- form*	*32.99*	*16.9*		
QPNBM	*2.38*	*2.49*	*2.59*	*3.78*	*12.2*			*2.88*	*9.32*
FAA-3-50	*2.26*	*2.36*	-	-	*5.05*			-	-

S16. Potential Vs time plot and hydroxide ion concentration with time plot

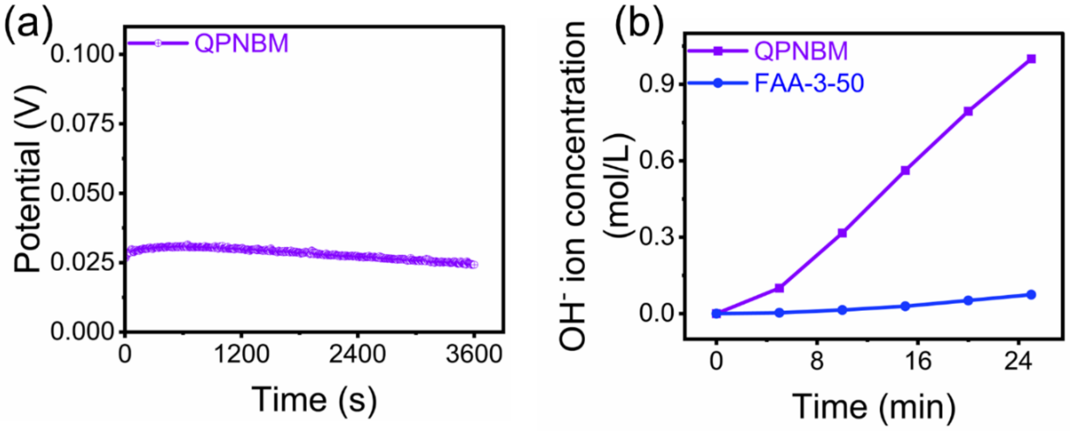

Figure S10. (a) The electrochemical potential curve of the QPNBM membrane in the concentration gradient of 1 M/0.1 M KOH and (b) Comparison of hydroxy ion permeability through QPNBM and FAA-3-50 membranes.

S17. Hydroxide ion transport number and ion diffusivity.

Table S3. The hydroxide ion transport number t_m and hydroxide ion permeability of QPNBM membrane.

Sample	$E_{measure}$ *(mV)*	ΔE_{jc}^{+} *(mV)*	$E_{membrane}$ *(mV)*	C_1 *(M)*	a_1	C_2 *(M)*	a_2	$t_m(OH^-)$	OH^- *ion permeability* 10^{-5} *(*cm^2S^{-1}*)*
QPNBM	*31.4*	*-5.82*	*37.22*	*0.1*	*0.733*	*0.01*	*0.0799*	*0.827*	*2.38*

$E_{meas} = \Delta E_{jc}^{+}$ without a membrane, $E_{meas} = \Delta E_{mem.} + \Delta E_{jc}^{+}$ with a membrane, 'a' is the activity coefficient, and 'C' is the concentration of the solution.

S18. ^{1}H NMR spectroscopy of PNBM polymer in long-term stability study

Spectroscopic analysis demonstrated a negligible vinyl proton peak after 1512 hours in a 1 M KOH solution at 80 °C, suggesting challenges in the quantitative analysis of piperidinium group degradation. The absence of a quaternary amine proton peak at ~8.5 ppm, in conjunction with the weak vinyl peak observed in the 1 M KOH environment, suggests an expedited Hofmann elimination process, which is further augmented by increased alkaline solution concentrations. Conversely, a significant vinyl proton peak emerged at approximately 6.5 and 4.7-5.4 ppm following 1775 h exposure to a 5 M KOH solution under identical thermal conditions. In conjunction with these observations, a water peak was detected alongside a methylene proton peak at 3.34 ppm. The degree of degradation of the piperidinium cation was evaluated by integrating the protonated amine signals with the intensity of aromatic protons. The degradation of the piperidine group was quantified at ~24%, which was accompanied by a corresponding decrease in OH^- ion conductivity of 30.7% in a 5M KOH solution after 1775 hours. Additionally, the ring-opening elimination of the piperidinium ring was estimated from the intensity of the vinyl protons (4.7-5.4 ppm & 6.5 ppm) relative to aromatic proton signals (7.2-8.2 ppm). The degradation proceeded via Hofmann elimination (~16%) and nucleophilic substitution reaction (~8%), indicating that Hofmann elimination is the predominant degradation mechanism.

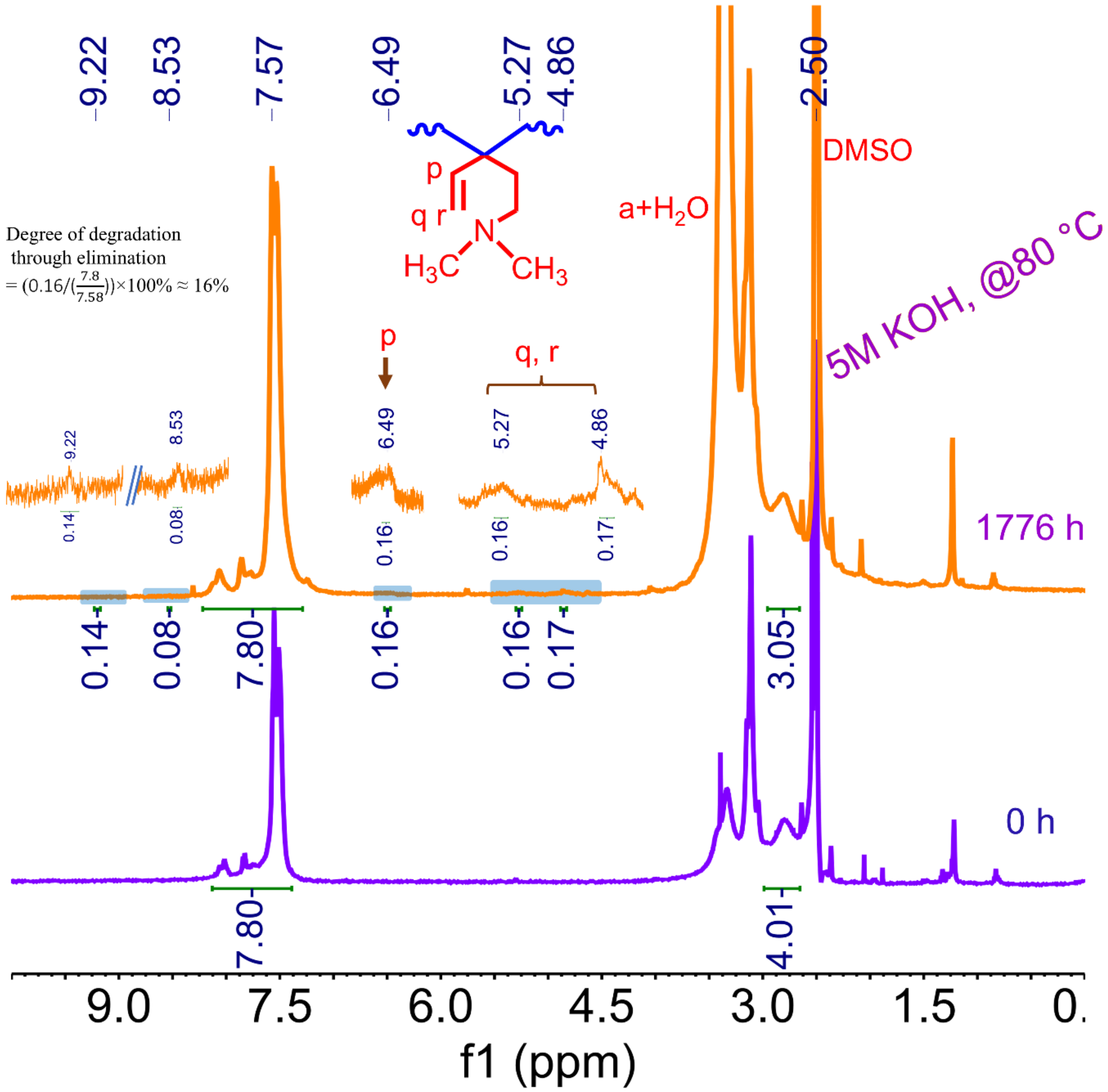

$$\text{Degree of degradation} = \frac{\text{Area of proton generate after ageing}}{\text{Area of the aromatic proton}} \times 100\%$$

$$\text{No. of aromatic proton per repeating unit} = \frac{(0.8*6)+(3*8)}{(3+0.8)} = 7.58$$

Figure S11. ^{1}H NMR spectra of the QPNBM membrane in DMSO d^6 before and after storage in 5 M KOH solution at 80 ºC for 1776 h.

S19. *AEMWE performance study*

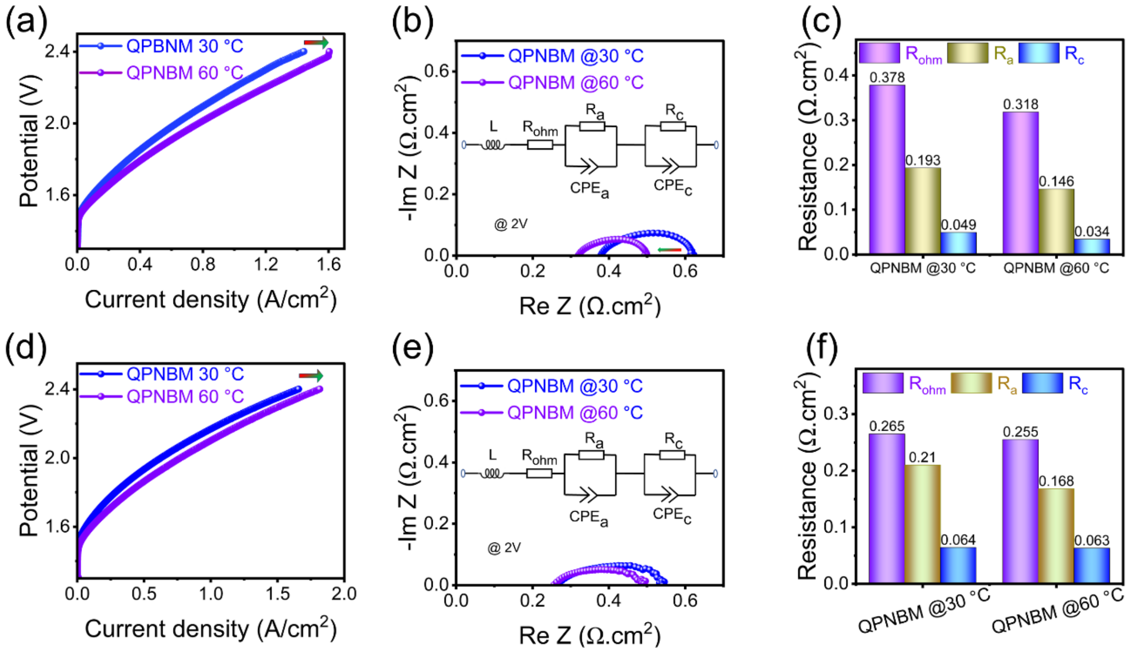

Figure S12. (a) Polarization curve of QPNBM membrane (50±5 μm) water electrolyzer (b) Nyquist plot and its equivalent circuit of the QPNBM members in AEMWE. (c) Resistance of the individual component obtained from equivalent circuit fitting. (d) The polarization curve of the QPNBM membrane, with a thickness of 35±5 μm, was evaluated in a water electrolyzer with an active area of 4 cm², achieving a maximum current density of 1.82 A/cm² at 2.4 V. (e) Nyquist plot and its equivalent circuit of the QPNBM membrane (35±5 μm) in AEMWE. (f) Resistance of the individual component, as determined through equivalent circuit fitting of the Nyquist plot (e).

S20. Table S4. A comparison of developed AEM performance with several membranes appeared in recent literature.

Membrane	**Anode**	**Cathode**	**Ionomer**	**Temp.**	**Performance 2.0 V (A/cm^2)**	**Solution**	**Stability**	**Thickness (µm)**	***Ref.***
QPNBM	IrO_2 1mg/cm^2	Pt/C 0.5 mg/cm^2	QPNBN	60°C	0.597	1M KOH	*470h 500mA/cm^2@1M KOH, 60°C*	*80± 5*	*This work*
QPNBM	IrO_2 3.5 mg/cm^2	Pt/C 0.8 mg/cm^2	QCBFM	80°C	1.68 @ 2.4V	1M KOH	*95h 500mA/cm^2@1M KOH, 60°C*	*50± 5*	*This work*
QPNBM	IrO_2 3.5 mg/cm^2	Pt/C 0.8 mg/cm^2	QCBFM	60°C	1.31 @2.4V	1M KOH	*95h 500mA/cm^2@1M KOH, 60°C*	*50± 5*	*This work*
QPNBM	IrO_2 3.5 mg/cm^2	Pt/C 0.8 mg/cm^2	QCBFM	60°C	1.82 @2.4V	1M KOH	-	*35± 5*	*This work*
FAA-3-50	IrO_2 1 mg/cm^2	Pt/C 0.5 mg/cm^2	FAA-3-50	60°C	0.476	1M KOH	-	*50± 5*	*This work*
FAA-3-50	IrO_2 3.5 mg/cm^2	Pt/C 0.8 mg/cm^2	QCBFM	60°C	0.497 @2.4V	1M KOH	*24h 500mA/cm^2@1M KOH, 60°C*	*50± 2*	*This work*
FAA-3-50	IrO_2 4 mg/cm^2	Pt/C 0.4 mg/cm^2	FAA3-Br	50°C	1.42	1M KOH (both electrodes)	-	50± 2	[9]
PISPVA46	IrO_2 ~2.01 mg/cm^2	Pt/C ~0.5 mg/cm^2	Nafion ionomer	60°C	0.547	0.5M KOH	80h 60°C 1.8V	55 ± 5	[10]
FOTFPh-TMA-C8	IrO_2 1.22 mg/cm^2	Pt/C 0.5 mg/cm^2	PFOTFPh-TMA (25 wt.%)	80°C	2	1M KOH	135h 200mA/cm^2 @1 M KOH, 80°C	23	[11]
HTMA-DAPP	IrO_2 2 mg/cm^2	PtRu/C 2 mg pt/cm^2	TMA-53	60°C	1.3	H_2O (both side flow)	170h 200mA/cm^2@H_2O, 60°C	26	[12]
PBP-Me	Ni-Foam	Pt/C 0.5 mg/cm^2	PiperION^{TM}	60°C	0.58	1M KOH	--	60	[13]

poly(vinyl benzyl methyl pyrrolidinium) -M-6#	NiFe	NiMo	Ionomer Free	80°C	1.2 @2.4 V	1M KOH (both side flow)	168h 500mA/cm^2@1M KOH, 80°C	80	[14]
GT 69	PbRuOx. 2 mg/cm^2	PtNi 2 mg/cm^2	GT 74	50°C	1 @1.95V	1 wt% KOH	5h 500mA/cm^2@1wt% KOH, 50°C	40	[15]
QPTTP-5%	IrO_2 2 mg/cm^2	Pt/C 1.5 mg/cm^2	QPTBP-5%	80°C	1.5 @2.2V	1M KOH	500h 500mA/cm^2@1M KOH, 60°C	30	[16]
PipPFTI-25	IrO_2 1 mg/cm^2	Pt/C 1 mg/cm^2	QPTBP-5%	60°C	0.838 @2.5V	1M KOH	15h 200mA/cm^2@1M KOH, 60°C	22	[17]
PAEN-DQA-35	IrO_2 2 mg/cm^2	Pt/C 2 mg/cm^2	-	30°C	0.521	1M NaOH	480h 500mA/cm^2@1M KOH, 30°C	35-45	[18]
PQP-100	IrO_2 1.5 mg/cm^2	Pt/C 1.3 mg/cm^2	PBP-67	85°C	1.544	1M KOH	402h 200mA/cm^2@1M KOH, 60°C	40	[19]
PAP100-dimethyl	Pt/C 0.4 mg Pt/cm^2	Pt/C 0.4 mg Pt/cm^2	PAP100-dimethyl	50°C	2 @ 3.1V	1M KOH	-	60 ± 5	[20]
C-IL-100	$NiFe_2O_4$ 2 mg/cm^2	NiFeCO 2mg/cm^2	-	80°C	0.88@ 2.2V	1M KOH	9.2 h 100mA/cm^2@1M KOH, 50°C	50 ± 5	[21]
QPBP-PX-15%	Ni–Mo–Al	Ni foam	-	80°C	1.1@ 2.1V	1M KOH	80 h 500mA/cm^2@6M KOH, 80°C	50	[22]

S21. Pore size distribution study

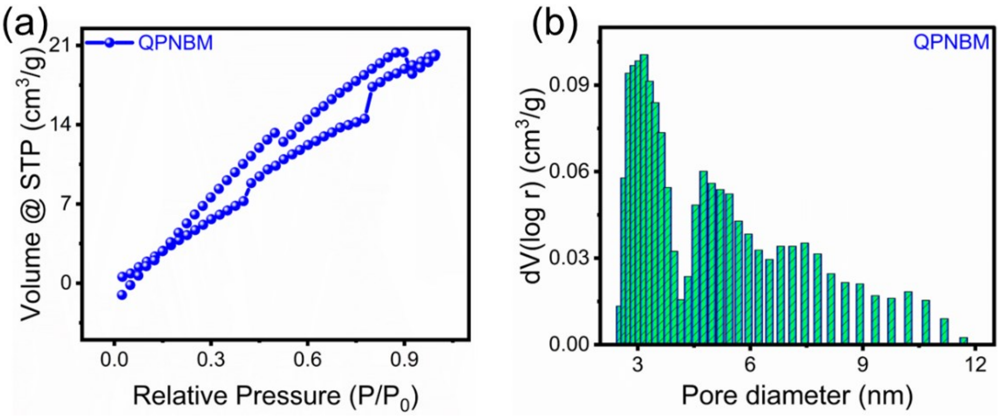

Figure S13. BET isotherm in figure (a) and pore size distribution in figure (b) for the QPNBM membrane in I^- form.

Table S5. Pore size, pore volume, and surface area of QPNBM membrane.

Ave. Pore diameter (nm)	*Pore volume (cm^3/g)*	*Surface area (m^2/g)*
3.168	*0.030*	*14.328*

S22. Ion permeability & Nyquist plot

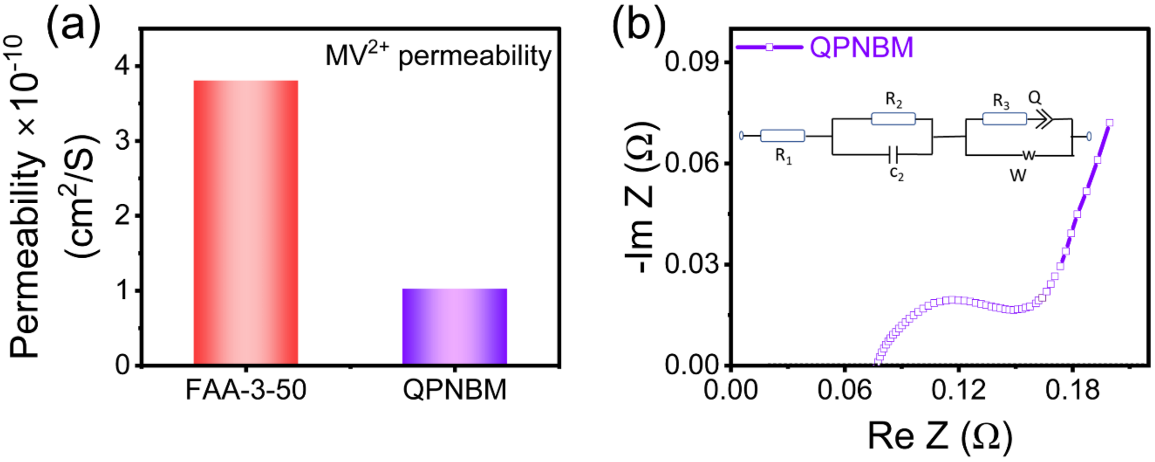

Figure S14. (a) The permeability study of methyl viologen in FAA-3-50 and QPNBM (90±5 μm) membranes. (b) Nyquist plot of battery cell assembled with MV/FcNCl in 2 M KCl and QPNBM membrane. The equivalent circuit of the corresponding Nyquist plot represents R_1,

R_2, and R_3, which are ohmic, anodic, and cathodic resistances. C_2, Q, and W represent capacitance, constant phase element, and workbag impedance, respectively.

S23. References

1 D. A. Klumpp, M. Garza, A. Jones and S. Mendoza, *J. Org. Chem.*, 1999, **64**, 6702–6705.

2 J. S. Olsson, T. H. Pham and P. Jannasch, *Adv. Funct Mater.*, 2018, **28**, 1–10.

3 J. Wang, Y. Zhao, B. P. Setzler, S. Rojas-Carbonell, C. Ben Yehuda, A. Amel, M. Page, L. Wang, K. Hu, L. Shi, S. Gottesfeld, B. Xu and Y. Yan, *Nat Energy.*, 2019, **4**, 392–398.

4 A. Shirole, P. M. Bakvand and P. Jannasch, *ACS Appl. Energy Mater.*, 2023, **6**, 7240–7249.

5 N. Chen, H. H. Wang, S. P. Kim, H. M. Kim, W. H. Lee, C. Hu, J. Y. Bae, E. S. Sim, Y. C. Chung, J. H. Jang, S. J. Yoo, Y. Zhuang and Y. M. Lee, *Nat. Commun.*, 2021, **12**, 2367.

6 Z. Li and Y. C. Lu, *Nat. Energy.*, 2021, **6**, 517–528.

7 M. Kumar, B. P. Tripathi and V. K. Shahi, *Electrochim Acta.*, 2009, **54**, 4880–4887.

8 J. E. Cha, M. H. Seo, Y. W. Choi and W. B. Kim, *J. Membr. Sci.*, 2021, **635**, 119471.

9 J. E. Park, S. Y. Kang, S. H. Oh, J. K. Kim, M. S. Lim, C. Y. Ahn, Y. H. Cho and Y. E. Sung, *Electrochim Acta.*, 2019, **295**, 99–106.

10 H. J. Park, S. Y. Lee, T. K. Lee, H. J. Kim and Y. M. Lee, *J. Membr. Sci.*, 2020, **611**, 118355.

11 R. Soni, S. Miyanishi, H. Kuroki and T. Yamaguchi, *ACS Appl. Energy Mater.*, 2021, **4**, 1053–1058.

12 D. Li, E. J. Park, W. Zhu, Q. Shi, Y. Zhou, H. Tian, Y. Lin, A. Serov, B. Zulevi, E. D. Baca, C. Fujimoto, H. T. Chung and Y. S. Kim, *Nat. Energy.*, 2020, **5**, 378–385.

13 T. Caielli, A. Raffaele, S. Bonizzoni, E. Sediva, A. Caprì, M. Santoro, I. Gatto, V. Baglio and P. Mustarelli, *J. Power Sources.*, 2023, **557**, 232532.

14 C. Rakousky, G. P. Keeley, K. Wippermann, M. Carmo and D. Stolten, *Electrochim Acta.*, 2018, **278**, 324–331.

15 G. Huang, M. Mandal, N. U. Hassan, K. Groenhout, A. Dobbs, W. E. Mustain and P. A. Kohl, *J. Electrochem Soc.*, 2021, **168**, 024503.

16 S. Zhang, X. Li, Y. Yang, J. Li, J. Zheng and S. Zhang, *J Membr. Sci.*, 2024, **698**, 122587.

17 Y. Wang, T. Ban, M. Guo and X. Zhu, *Int. J. Hydrogen Energy.*, 2024, **49**, 1123–1133.

18 J. Hu, K. Chen, X. Zhang, J. Qian, J. Li, Q. Ren and C. Wang, *Int. J. Hydrogen Energy.*, 2024, **62**, 498–509.

19 M. Liu, X. Hu, B. Hu, L. Liu and N. Li, *J. Membr. Sci.*, 2021, **642**, 119966.

20 V. D. C. Tinh, V. D. Thuc, Y. Jeon, G. Y. Gu and D. Kim, *J. Membr. Sci.*, 2022, **660**, 120903.

21 X. Wang and R. G. H. Lammertink, *J. Mater. Chem. A.*, 2022, **10**, 8401–8412.

22 Z. Zheng, B. Xue, J. Yao, Q. He, Z. Wang and J. Yan, *Materials Horizons., 2024,* ***11****, 6117*.